Science of the Total Environment 900 (2023) 165790

Contents lists available at ScienceDirect

Science of the Total Environment

journal homepage: www.elsevier.com/locate/scitotenv

Water activity in subaerial microbial biofilms on stone monuments

A. Tenore [a], Y. Wu [b], J. Jacob [c], D. Bittermann [c], F. Villa [d], B. Buttaro [e], I. Klapper [b,*]

[a] Department of Mathematics, Università degli Studi di Napoli Federico II, Naples, Italy
[b] Department of Mathematics, Temple University, Philadelphia, PA, United States of America
[c] U.S. National Park Service, North Atlantic-Appalachian Region, Historic Architecture, Conservation, and Engineering Program, United States of America
[d] Department of Food, Environmental and Nutritional Sciences, Università degli Studi di Milano, Milan, Italy
[e] Sol Sherry Thrombosis Research Center, Katz School of Medicine, Temple University, Philadelphia, PA, United States of America

ARTICLE INFO

Editor: Patricia Sanmartin

Keywords:
Subaerial biofilm
Outdoor stone monuments
Water activity
Mathematical models

ABSTRACT

Stone monuments can be difficult environments for life, particularly with respect to liquid water access. Nevertheless, microbial communities are found on them with apparent ubiquity. A variety of strategies for access to liquid water have been proposed. Regardless of their water-retention mechanisms details, though, we argue that water activity (a key indicator for cell viability) is constrained by environmental conditions, largely independently of community structure, and is predicted by the local temperature and relative humidity. However, direct measurement of water activity in SABs, particularly those growing on stone surfaces, is difficult. A method for estimating water activity within SABs is presented that uses a minimally invasive combination of conservative sampling, weather data, confocal imaging, and mathematical modeling. Applying the methodology to measurements from the marble roofs of the Federal Hall National Memorial and of the Thomas Jefferson Memorial, estimations are made for water activity in their subaerial stone communities over the course of an approximately one year period.

1. Introduction

Surfaces of outdoor stone monuments can be viewed as mosaics of air-exposed mineral substrata that are subjected to various environmental stresses. Despite being oligotrophic and polyextreme habitats, these stone-air interfaces support growth of subaerial biofilms (SABs), which are interactive microbial communities embedded within an extracellular polymeric matrix (EPM) (Adhikary and Kovacik, 2010; Gaylarde et al., 2012; Song et al., 2012; Stupar et al., 2012; Videla et al., 2000). The keystone species of SAB communities are often hardy oxygenic phototrophs, specifically cyanobacteria or algae, capable of converting inorganic carbon into organic, biologically available carbon through processes of carbon fixation. These phototrophs may then supply a surrounding community of chemoorganotrophs with reduced, organic carbon, and over time it is expected that the entire community will gradually approach a quasi-steady state in which microbial inhabitants maintain a stable coexistence and experience a slow, gradual pace of ecological change. Details of the resulting SABs are determined by interplay between local chemical and physical constraints which generate an environment with limited resource availability (Villa et al., 2015), minimal microbial competition within SABs (Gorbushina, 2007), and the selection of microorganisms that exhibit resistance to multiple stresses (Gorbushina, 2007). Together, these factors contribute to the ability of SABs to push themselves to the limits of viability by establishing stable, persistent, self-sustaining, and functionally balanced microbial communities, wherein nutrients and energy are efficiently cycled and cells are protected from external injuries (Zanardini et al., 2018; Villa and Cappitelli, 2019).

When atmospheric carbon dioxide and light are in adequate supply for photosynthesis, liquid water will commonly be the limiting factor in this quasi-steady state with respect to community activity. Thus, flux of water through the system is central to community sustainability, as it supports photosynthesis and the generation of energy required to maintain the entire community (Lange et al., 1984). We should keep in mind that a significant portion, potentially up to 97 %, of (fully hydrated) biofilm is composed of water (Sutherland, 2001). Binding and movement of water within the EPM play crucial roles in diffusion processes taking place within biofilms (Quan et al., 2022). Hence, liquid water is necessary for the exchange of molecules (including metabolites, gases, waste products, salts, biocides, and signaling molecules) between community inhabitants, and for the basic function and structural integrity of the EPM (Flemming et al., 2023). However, water content of

* Corresponding author.
E-mail address: klapper@temple.edu (I. Klapper).

https://doi.org/10.1016/j.scitotenv.2023.165790
Received 27 March 2023; Received in revised form 30 June 2023; Accepted 23 July 2023
Available online 28 July 2023

a SAB does not reflect its water activity, which is a measure of the amount of free, liquid water available for microbial growth and metabolic activity (Allen Jr., 2018). For example, water molecules within a SAB may be tightly bound to the EPM, resulting in limited interaction with cells and the surrounding environment (Quan et al., 2022) and, consequently, despite the presence of a substantial amount of water, its restricted accessibility defines the SAB as having low water activity. In this way, water activity becomes a key parameter to assess SAB metabolic activity and evaluate impact on stone surfaces.

Unsurprisingly, the presence of SABs is frequently associated with stone deterioration via water-mediated weathering (Alves et al., 2021; Sass and Viles, 2022), and water activity too should be taken into account. As an example, high water activity may affect the photosynthetic activity of SAB-dwelling microorganisms and, consequentially, the pH of the extracellular environment. The initial raising of pH resulting from the lowering of CO2 levels, and the later decrease of pH through the release of partially reduced organic matter and subsequent bursts of respiration (McNamara and Mitchell, 2005), can induce dissolution and/or precipitation reactions of carbonate minerals (Zhang and Klapper, 2010). These reactions can lead to erosion of the underlying stone (Liu et al., 2020). Water activity of SABs can also provide insights into the direction of water movement, e.g., a dry atmosphere draws moisture from a relatively high water activity SAB, which may in turn pull moisture from the lithic substrate. Wetting and drying cycles can cause the accumulation of salts within the stone pores. The subsequent crystallization of these salts may contribute to internal stress and crack formation, ultimately resulting in surface delamination and damage (Li and Gu, 2022).

To best retard erosion of stone monuments, understanding the availability and movement of water within its stone-SAB-atmosphere ecosystem is fundamental and essential. The majority of methods used to measure water activity in biological samples rely on determining the equilibrium moisture content (e.g., manometric, gravimetric, psychrometric, and hygrometric methods) (Rödel, 2001). In this context, "equilibrium" refers to the point at which the water activity of the sample thermodynamically equilibrates with the relative humidity of the air contained within a sealed measuring chamber impermeable to water vapor. This is not a realistic description of conditions on stone monuments. Further, it is important to note that, currently, there are no existing methods that provide non-destructive and in situ measurements of water activity in SABs. In fact, there is a sparsity of data regarding water activity in biofilms in many different settings, not limited to SABs. Thus, there is a need to provide means for practical and reliable measurement of water activity in SABs.

The goal of this study, then, is to propose a method to estimate water activity that is suitable for minimally invasive use in the field under varying local environmental conditions, based on a mathematical model as described below. To do so, we describe how water activity – a key indicator of water availability – is constrained by environmental conditions, and is predicted by local temperature, relative humidity and SAB thickness, irrespective of the specific microbial community composition. The resulting mathematical model offers a straightforward estimation of SAB water activity by utilizing easily accessible parameters, thereby avoiding the need for sample collection and ex-situ analyses. This is particularly advantageous when working with monuments, where preservation is paramount and invasive sampling and analytical procedures are discouraged or disallowed. To illustrate our approach, we conducted a study using physical and biological data gathered over a one-year period from the marble roofs of two iconic monuments: the Thomas Jefferson Memorial in Washington, D·C., and Federal Hall National Memorial in New York, N.Y. By analyzing the resulting data, we estimated the water activity within the SABs inhabiting these monuments and compared water activity conditions and microbial communities between the two sites. Results of this study suggest that this new mathematically based framework will offer valuable insights into the complex water dynamics within SABs, contributing to the advancement of microbial ecology research and improving sustainable conservation practices for cultural heritage.

2. Materials and methods

Later (in Section 3) we present a physically-based mathematical model of SAB water activity as a function of certain weather data (temperature and relative humidity values as detailed below) as well as of SAB thickness. For that purpose, we describe field sites and measurement and estimation methods in the subsections below. For completeness, we have also verified the presence of cyanobacteria-rich SABs at the field sites, see Supplemental Material, though the species make-up of the SAB is not a model variable.

2.1. Study sites and weather data

Studies were conducted at two sites. The Thomas Jefferson Memorial (TJM) is in Washington, DC, adjacent to the Tidal Basin, and was constructed between 1938 and 1943. Its marble came from the Imperial Danby Quarry in Rutland County, in central Vermont, and is characterized by fine-grain calcite crystals. Although in a large city, the memorial is situated in an open environment with relatively unimpeded exposure to sun (other than self-shading) as well as radiative heating and cooling (Fig. 1). The second site, Federal Hall National Memorial (FH), is in New York City, on Wall Street at the southern tip of Manhattan. It was constructed between 1834 and 1842 as a U.S. Custom House. Marble for the roof was quarried in the village of Tuckahoe, in Westchester County, NY., and is characterized by coarse-grain calcite and dolomite crystals. Unlike TJM, the building is surrounded by significantly taller buildings which restrict exposure to direct sun, and the roof is subject to radiative and reflective heating from the surrounding buildings (Fig. 1).

Weather-related data was collected from the roofs of the TJM and FH between August of 2015 and August of 2016. Relative humidity and temperature were recorded adjacent to the stone, i.e., measurement devices were placed in direct contact with the stone surface, see Fig. 1, and in nearby ambient air using Hygrochron DS1923 temperature and humidity ibutton loggers, in duplicates (Maxim Integrated, San Jose, CA). Note that only temperature was recorded in the ambient air. Light intensity was measured using Li-Cor LI-190 quantum sensors which measures photosynthetic active radiation in the 400–700 nm waveband, with data recorded on LI-1500 Dataloggers (LI-COR, Lincoln, NE). Rain was measured using RG3 Hobo Pendant Event Data Loggers with tipping bucket rain gauges (Onset, Bourne MA). Also, ambient air condensation measurements were made using HOBO S-LWA-M003 leaf-wetness sensors with H21–002 Micro Station Data Loggers (Onset, Bourne MA). See Fig. 1. Full data sets are included in the Supplemental Material.

2.2. Confocal imaging

We hypothesize that SAB depth may impact SAB water activity (see mathematical model below), and so confocal imaging was employed to measure SAB thickness. To create the confocal images, samples were obtained by gently scraping with a sterile scalpel from the marble surfaces of the roof of FH, April 29, 2022, and the dome of TJM on May 18, 2022. For imaging, e.g., Fig. 2, approximately 1–3 mg of stone particles were distributed onto the adhesive side of a 2 × 1 cm fungi tape placed on a glass slide. PBS (100 ml total volume) containing Syto9 (0.3 ml/100 ml, Invitrogen), Biotium-labelled WGA Wheat Germ Agglutinin (4.7 ml/100 ml, Sigma) was applied to the adhesive tape. A 1.5 optic coverslip (20 × 22 mm) was placed on the tape, and the sides were sealed with care being taken to create surface tension between the slide and the glass to stabilize movement but not so firmly as to cause cell lysis. Syto9 has green fluorescence and was used for staining the DNA of cells and eDNA. Biotium-labelled WGA has blue fluorescence and was used for staining glycoproteins in 1,4-*N*-acetylglycosamine-linked residues common in heterotrophic bacteria matrix, but does not bind most

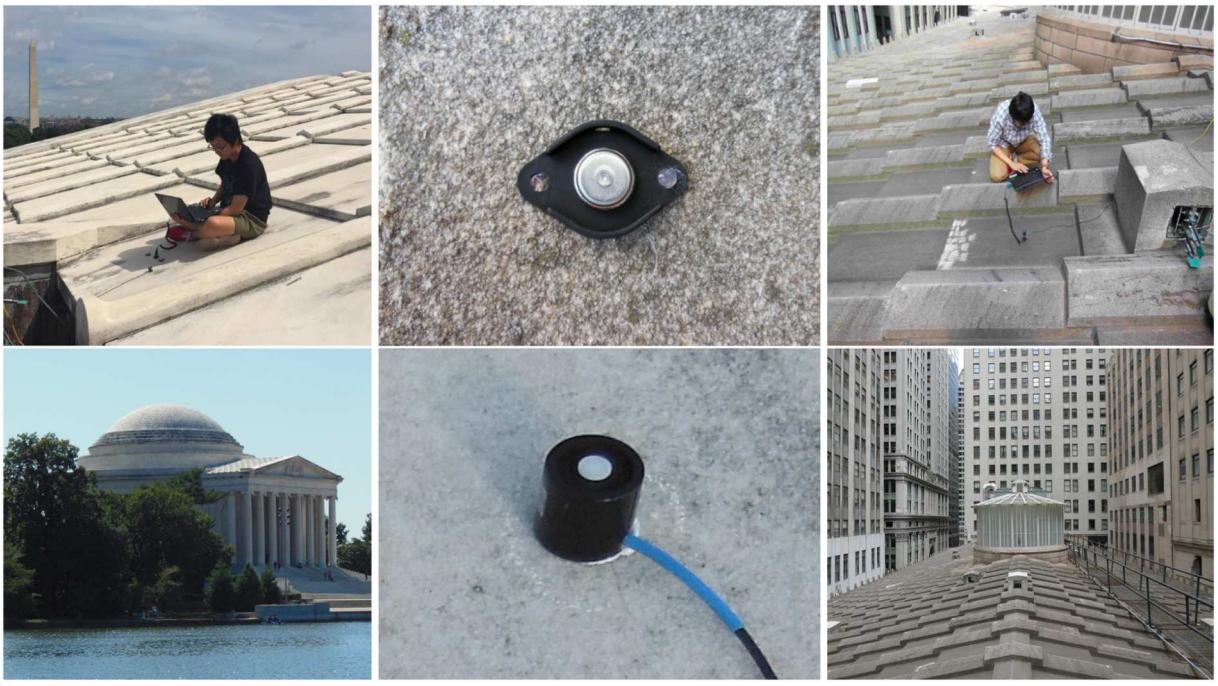

Fig. 1. Field sites. (Top left) roof of the TJM portico, Y. Wu downloading data from an ibutton. (Bottom left) TJM, front view with portico. (Top middle) close-up from the roof of FH of an ibutton with security mount. (Bottom middle) close-up from the roof of TJM of a light meter. (Top right) roof of FH, Y. Wu downloading data from an ibutton, adjacent to scraping sampling locations. Note that a leaf-wetness sensor is visible (green square, right side). (Bottom right) FH roof, note the surrounding urban canyon.

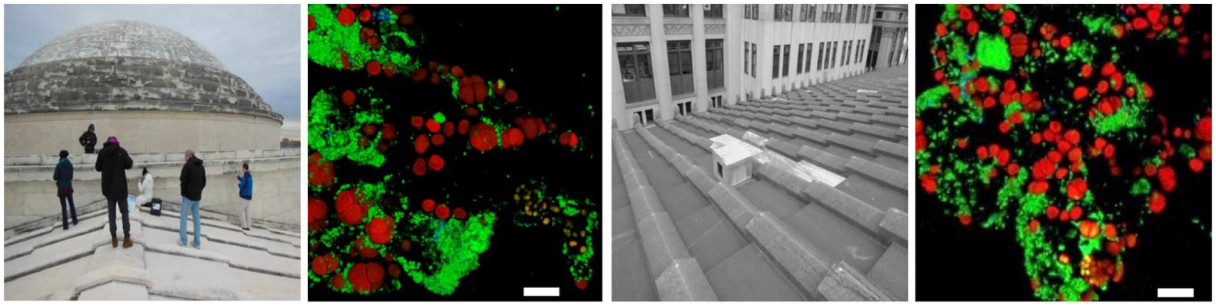

Fig. 2. Subaerial biofilms. Left: TJM portico and dome, note chronic biofilm-associated dark areas, with a data collection team on the portico roof. Middle left: sample from a SAB inhabiting the TJM portico. Middle right: FH roof with, again, biofilm-associated dark areas. Right: sample from a SAB inhabiting the FH roof with (red) cyanobacterial autoflorescence and (green) florescent DNA stain. Scale bars = 20 μm.

cyanobacterial matrix materials (Zippel and Neu, 2011). Photosynthetic machinery of cyanobacteria emits a red fluorescence when excited by a 561-nm laser.

Imaging was done using a Leica SP5 microscope equipped with a TCS confocal system using a 63× objective at 1024 × 1024-pixel resolution. Syto9 was excited with a 488-nm laser, and emission was measured from 510 to 545 nm. Biotium-WGA was excited with a 405-nm laser, and emission was measured from 410 nm to 460 nm was measured. Photosynthetic machinery of cyanobacteria was excited with a 561-nm laser, and emission was measured from 620 nm to 735 nm.

2.3. Measurement of SAB thickness

Using confocal images as described in Section 2.2, we estimated SAB thicknesses as follows. Images, were imported into ImageJ (Rasband, 2018), and 3D projections were produced using 3D Viewer (Ollion et al., 2013). Because biofilms form on particles, the angle of a transverse z-plane changes with location, preventing the use of automated tools that estimate biofilm thickness from the base of the image taken of a biofilm on a flat surface. To determine the thickness of biofilms on particles, images were imported into ImageJ and visualized in 3D using 3D viewer. Images were rotated to find correct orientation of the Z plane. Using the multi-point tool, couples of points (x_1, y_1, z_1) and (x_2, y_2, z_2) were manually chosen, accounting for the top and bottom of the SAB layer. Then, the SAB thickness was computed as the distance $\sqrt{(x_1 - x_2)^2 + (y_1 - y_2)^2 + (z_1 - z_2)^2}$ (see Fig. 3). The SAB mounts consisted of random selection of particles from the material collected across the 3 cm × 2 cm area that was scraped. Since we were interested in growth constraints, maximum depths were measured. Due to their spatial arrangements, some SABs yielded multiple points that could be accurately measured such as the example in Fig. 3, while others yielded only a single good measurement. For TJM, six images were analyzed yielding 6, 5, 3, 2, 1, and 1 measurements for a total of 18 data points. For FH, again six images were analyzed yielding 5, 5, 4, 3, 2, 1, 1 for a total of 20 data points.

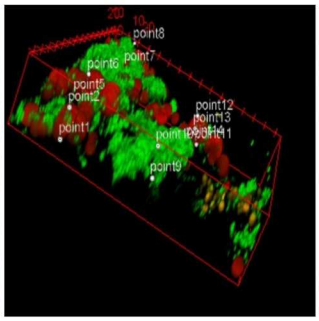

	x [μm]	y [μm]	z [μm]	Thickness [μm]
Pt 1	32.6	154.2	28.5	16.0
Pt 2	31.3	152.1	12.7	
Pt 5	19.4	113.9	19.3	14.4
Pt 6	23.0	111.2	5.6	
Pt 7	17.4	5.8	18.3	17.4
Pt 8	17	0.3	1.8	
Pt 9	88.8	144.9	21.4	15.6
Pt 10	85	142.7	6.4	
Pt 11	100.2	76.7	15.2	15.9
Pt 12	93.7	74.5	0.9	
Pt 13	92.3	40.9	17.8	11.5
Pt 14	90.5	37.9	28.8	

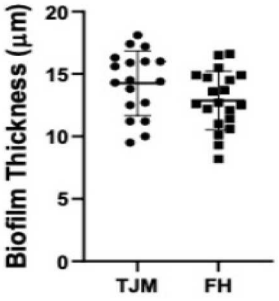

Fig. 3. Sampling. (Left) main sampling site at FH, 08/09/2016. (Middle left) Multi-point selection on a confocal microscope image of a TJM biofilm colony (length and width are 150 μm, height is 63 μm) with (red) cyanobacterial autoflorescence and (green) florescent DNA stain. (Middle right) Locations of the points in local coordinates x, y, and z on the confocal image in μm with calculated thicknesses. During placement of the second point care is taken to maintain the x and y position as closely as possible to the first point so the measured difference will be in the transverse (to the SAB) direction. Thickness is then measured using the formula given in the text. (Right) Estimated SAB thicknesses from TJM and FH samples. Thick horizontal bars are means and thin horizontal bars delineate one standard deviation.

2.4. Estimation of ambient relative humidity

Ambient relative humidity was estimated by using the data on temperature and humidity adjacent to the stone together with temperature in the ambient air. Assuming the water content in the ambient air to be the same as that adjacent to the stone (so that water vapor partial pressure P_{WV} is also the same), ambient relative humidity can be estimated from the relation

$$\mathrm{RH} = \frac{P_{\mathrm{wv}}}{P_{\mathrm{sat}}(T)} \tag{1}$$

with $P_{\mathrm{sat}}(T) =$ equilibrium water vapor saturation pressure over pure water. Eq. (1) combined with the Magnus formula

$$P_{\mathrm{sat}}(T) = a e^{\frac{b(T-273.15)}{c+T-273.15}}$$

(with coefficients $a = 610.94$ Pa, $b = 17.625$, $c = 243.04$°C, determined empirically for temperature range $-40 < T < 50$ °C (Alduchov and Eskridge, 1997)) results in relation

$$RH_a = \frac{e^{\frac{b(T_s-273.15)}{c+T_s-273.15}}}{e^{\frac{b(T_a-273.15)}{c+T_a-273.15}}} RH_s,$$

where RH_a is the ambient relative humidity, RH_s is the relative humidity adjacent to the stone, T_a is the ambient air temperature, and T_s is the stone temperature.

2.5. The thermal diffusive boundary layer

Between the stone surface and the ambient air, there is a thin, insulating region called a thermal boundary layer; the thicker the layer, the slower that heat is transported between them and hence the greater the temperature differences. It occurs because, adjacent to surfaces, air velocity generally takes a laminar, shear form as it transitions from zero at the surface to ambient air flow. In this laminar layer (whose thickness is related to fluid kinematic viscosity ν), flow is parallel to the surface so transverse heat transport is not assisted by advection and hence largely depends on relatively slow molecular diffusion, thus forming the thermal diffusive boundary layer. Following (Schlichting, 1955), we discuss here the estimate made of the thermal diffusive boundary layer depth ℓ, which is related to the laminar velocity boundary layer depth δ through the Prandtl number $Pr = \nu/k_a$ via

$$\ell = \delta Pr^{-1/3},$$

where ν is the fluid kinematic viscosity and k_a the thermal diffusivity. In the case of air, $\nu = 1.47{\cdot}10^{-5}$ m^2/s and $k_a = 1.9{\cdot}10^{-5}$ m^2/s and so, consequently, $\ell = 1.09\delta$.

The velocity boundary layer depth δ adjacent to a flat boundary (such as the marble roofs considered here) is determined by the local aerodynamic conditions, i.e., the near-surface bulk air flow conditions. We model this using the theory of boundary layers over flat plates. In the case of a no-slip boundary condition on the plate and following the common convention of defining δ to the distance from the plate at which air speed reaches $0.99U$, where U is the bulk field air speed, then the approximation

$$\delta = \frac{5x}{\sqrt{Re}}$$

is applied, where Re is the Reynolds number and x is the distance along the plate.

Using typical wind speeds $0.5 < U < 4$ m/s in the Washington D.C (Reagan National Airport weather station), and New York City area (New York City Central Park weather station), we plot estimated thermal diffusive boundary layer thicknesses in Fig. 4. Study sites in those two cities, TJM and FH, respectively, have topographical obstructions within approximately 0.5 m, so that we estimate that ℓ will generally be less than about 2 cm. As a representative value, we have set $\ell = 1$ cm.

3. Theory

3.1. Physics of relative humidity and water potential

Generally, rain provides an SAB with an occasional and ephemeral source of water. However, water vapor in the air is consistently available, and liquid water can be induced to form thin layers on subaerial surfaces via hydrophilic and hygroscopic SAB components. That is, an SAB, preferring to be well hydrated, will exhibit a tendency to draw in water, or water vapor, in a similar manner as, say, a quantity of salt would do so. We identify this tendency, physically, as a microbially-associated osmotic tension. The forces acting on water held within a porous medium are often grouped in three categories: chemical interactions between water and non-dissolved or solid material (termed matric forces in the soil literature (Day et al., 1967)), e.g., water-EPS interactions, osmotic force arising from dissolved components, e.g., salts, and physical body forces, e.g., gravity. We neglect body forces under the supposition that they have negligible effect on thin SABs and inclusion wouldn't change the principle conclusion, and group the other two as generalized osmotic forces. These include both those soluble components, e.g., salts, and insoluble components, e.g., EPS, of the stone-SAB system that might attract water.

To quantify, consider a one-dimensional model as in Fig. 5, consisting of a mixed biofilm-liquid water layer ($0 < z < h$) resting on impermeable stone ($z = 0$) and below a region of moist air ($z > h$). In an immediately adjacent parcel of air, the water potential (Potts, 1994)

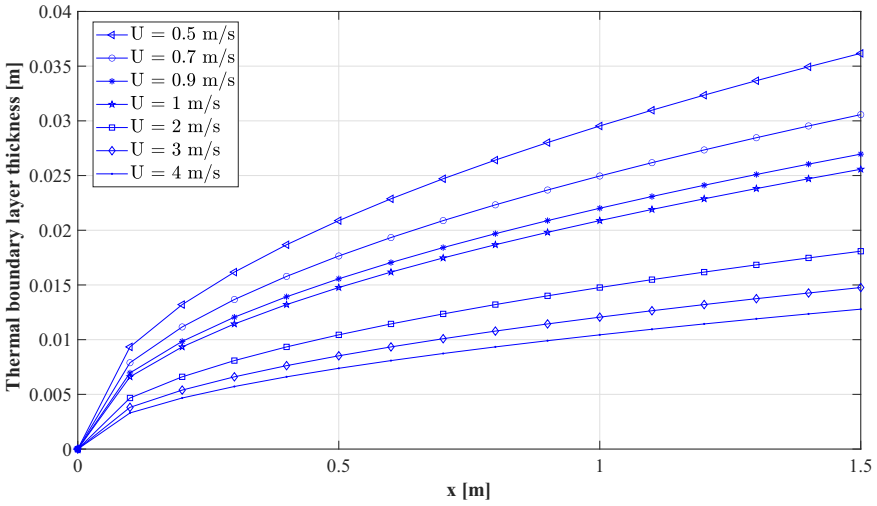

Fig. 4. Thermal boundary layers. Estimation of the thermal boundary layer thickness over a flat stone surface, for different values of bulk field air speed U and distance x from the leading edge.

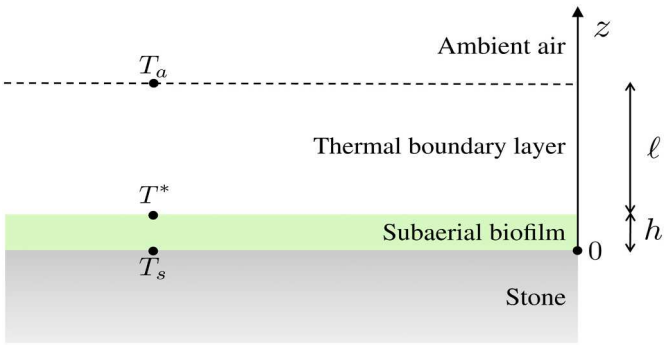

Fig. 5. Model diagram. An SAB (green layer, $0 < z < h$) forms on impermeable stone ($z \leq 0$) at temperature $T = T_s$. Heat transports diffusively. Ambient air ($z \geq h$) temperature is $T = T_a$ for $z \geq h + \ell$ with a thermal boundary layer $h < z < h + \ell$. At steady state, the temperature at the SAB-air interface must be at the SAB dew point temperature T^*, determining thickness h according to Eq. (6).

$$\psi_{\text{vap}}(T) = (\mathcal{R}T/\overline{V}_{\text{W}})ln\text{RH} \tag{2}$$

must approximately match that of the SAB water potential

$$\psi_{\text{SAB}} = -\Pi \tag{3}$$

at steady state. Here $\mathcal{R}$ is the universal gas constant, T (Kelvin) is air temperature, and $\overline{V}_{\text{W}}$ is the partial molal volume of water. Relative humidity RH (at temperature T) is defined as in (1) . The quantity Π is defined to be a combined SAB osmotic and matric tension (Potts, 1994), arising from solutes as well as from macromolecules and other non-dissolved quantities, which we term a generalized osmotic potential. $\Pi(w)$ is a decreasing function of liquid water volume fraction $w \in [0, 1]$ in the SAB with $\Pi(1) = 0$ and $lim_{w\to 0}\Pi(w) = \infty$. Note then that the SAB dew point temperature, i.e., the temperature $T^* = T^*(\Pi)$ at which $\psi_{\text{vap}}(T^*) = \psi_{\text{SAB}}$, is higher than the "atmospheric" dew point temperature. That is, assuming that SABs are water-attracting, then water condensation will occur on SABs at higher temperatures than the standard dew point. Noting that SAB temperature is close to the adjacent stone and air temperatures, then, roughly speaking, the SAB will pull water condensate from the adjacent air, thus changing osmotic tension Π until $T^*(\Pi)$ allows a steady state.

Introducing water activity a_{w} (in the SAB), defined by (Nobel, 2020)

$$ln a_{\text{w}} = \frac{\overline{V}_{\text{W}}}{RT}\psi_{\text{SAB}} \tag{4}$$

note thus that, at the SAB-air interface,

$$a_{\text{w}} = \text{RH} \tag{5}$$

at steady state, where RH is measured in the parcel of air adjacent to the SAB. Indeed, relation (5) has been used to measure water activity in brine communities, e.g. (Benison et al., 2021).

Two remarks. First, water potential is computed with respect to a system temperature, here set to be the temperature at the SAB-air interface. (Note that, in the case that the SAB is thin, temperature is approximately constant in the SAB layer.) More typically, water potential is introduced in temperature-homogeneous systems; however, it is still well-defined here, and is continuous, when the system is at steady state. Second, we are implicitly supposing a quasi-steady state with respect to water since environmental conditions change slowly; there may be circumstances where this assumption fails, e.g., periods of rain.

Water activity is a key parameter in viability and growth of microorganisms (Brown, 1990), and here we have noted its direct connection, in the case of SAB communities, to relative humidity. That is, while generalized osmotic tension Π can impact total amount of available liquid water, possibly in complicated and difficult to measure ways, it does not have a direct role in determining water activity, at least at steady state. Rather, water activity is instead determined by environmental conditions. That is, SAB systems can make themselves "sticky" to liquid water in various ways, e.g., via soluble compounds such as salts present in the stone, or hydrophilic insoluble elements such as might be found in EPS, that attract water by providing a low water potential environment. However, precisely because of that low potential, such water is not freely available for chemical reaction elsewhere. Still, though such liquid water can be useful, e.g., for structural integrity and other purposes (Brown, 1990), even possibly at lower water activity levels, many chemical processes require high water activity to proceed. Note that keeping even low activity water might be energetically expensive particularly in dry conditions, but as the inputs to photosynthesis, namely water and CO_2 are available, in principle there may be availability of the energy needed to do so.

3.2. A mathematical model of SAB water activity

Water activity constraints have consequences for SAB community structure. We thus construct a mathematical model able to estimate

water activity a_w, given some basic data as described below. Referring to Fig. 5, the temperature profile is determined by diffusive heat transport between stone and ambient air, with a biofilm layer of thickness h and a diffusive thermal layer of thickness ℓ in between. As SAB thickness h and boundary layer thickness ℓ are small (we use estimate $\ell = 1$ cm, see Section 2.5), we can assume that the temperature $T(z)$ maintains a quasi-steady profile and so satisfies the time-independent heat equation $k_a T^{'} = 0,\ 0 < z < h$, $k_b T^{'} = 0,\ h < z < h + \ell$, where k_a and k_b are thermal diffusivities of air and SAB, respectively (we use $k_a = 1.9{\cdot}10^{-5}$ m^2/s, and $k_b = 1.4{\cdot}10^{-7}$ m^2/s), and with Dirichlet conditions $T(0) = T_s$, $T(h + \ell) = T_a$. Continuity conditions $[T] = [kT^{'}] = 0$ hold at the interface $z = h$. SAB layer thickness h can be determined using the additional steady state condition $T(h) = T^*$ at the air-liquid interface $z = h$, with result

$$h = \ell \frac{k_b}{k_a} \frac{T^* - T_s}{T_a - T^*}. \tag{6}$$

Formula (6) is valid for $T_s \le T^* < T_a$ or $T_a \le T^* < T_s$; these inequalities are required thermodynamically. If it were the case that T^* lay below the temperature interval I formed by T_s and T_a, then an SAB on the stone surface would release liquid water, thereby increasing generalized osmotic tension Π, until $T^* \in I$. The reverse process, namely liquid water absorption, would occur if T^* were to be above I. Note that at hydrostatic steady state, Π is necessarily constant in the SAB layer.

The SAB dew point temperature T^* is determined by generalized osmotic tension as follows. First, note that, at the SAB-air interface, $\psi_{vap} = \psi_{SAB}$ at steady state, i.e., from eqs. (2) and (3),

$$\frac{RT^*}{\overline{V}_W} ln \frac{P_{wv}}{P_{sat}(T^*)} = -\Pi.$$

From Eq. (1), $\mathrm{RH}_a = P_{wv}/P_{sat}(T_a)$, and thus

$$\mathrm{RH}_a P_{sat}(T_a) = e^{-\frac{\overline{V}_W}{RT^*}\Pi} P_{sat}(T^*). \tag{7}$$

Saturation pressure $P_{sat}(T^*)$ is monotone increasing in T^* and hence steady state formula (7) can be inverted to solve for T^* in terms of RH_a, T_a, and Π (or, alternatively, a_w).

We derive an explicit approximation to T^* as follows. Replacing generalized osmotic tension Π by water activity a_w (using eqs. (3) and (4)) and applying the Magnus formula (see Section 2.4) to approximate saturation pressure, we obtain from relation (7) the approximate formula

$$T^* = \frac{c\left(ln\frac{\mathrm{RH}_a}{a_w} + \frac{b(T_a - 273.5)}{c + T_a - 273.5}\right)}{b - \left(ln\frac{\mathrm{RH}_a}{a_w} + \frac{b(T_a - 273.5)}{c + T_a - 273.5}\right)} \tag{8}$$

for T^* as a function of measured ambient relative humidity RH_a, ambient air temperature T_a, and generalized osmotic tension Π. Combining results (6) and (8) results in a relation $a_w = f(h, T_s, T_a, RH_a)$, independent of SAB dew point temperature T^* (and generalized osmotic tension Π). Note: this is the water activity at the top of the SAB layer, cf. Fig. 5. Water activity varies with temperature, recall Eq. (4), and so will vary a bit across the SAB layer.

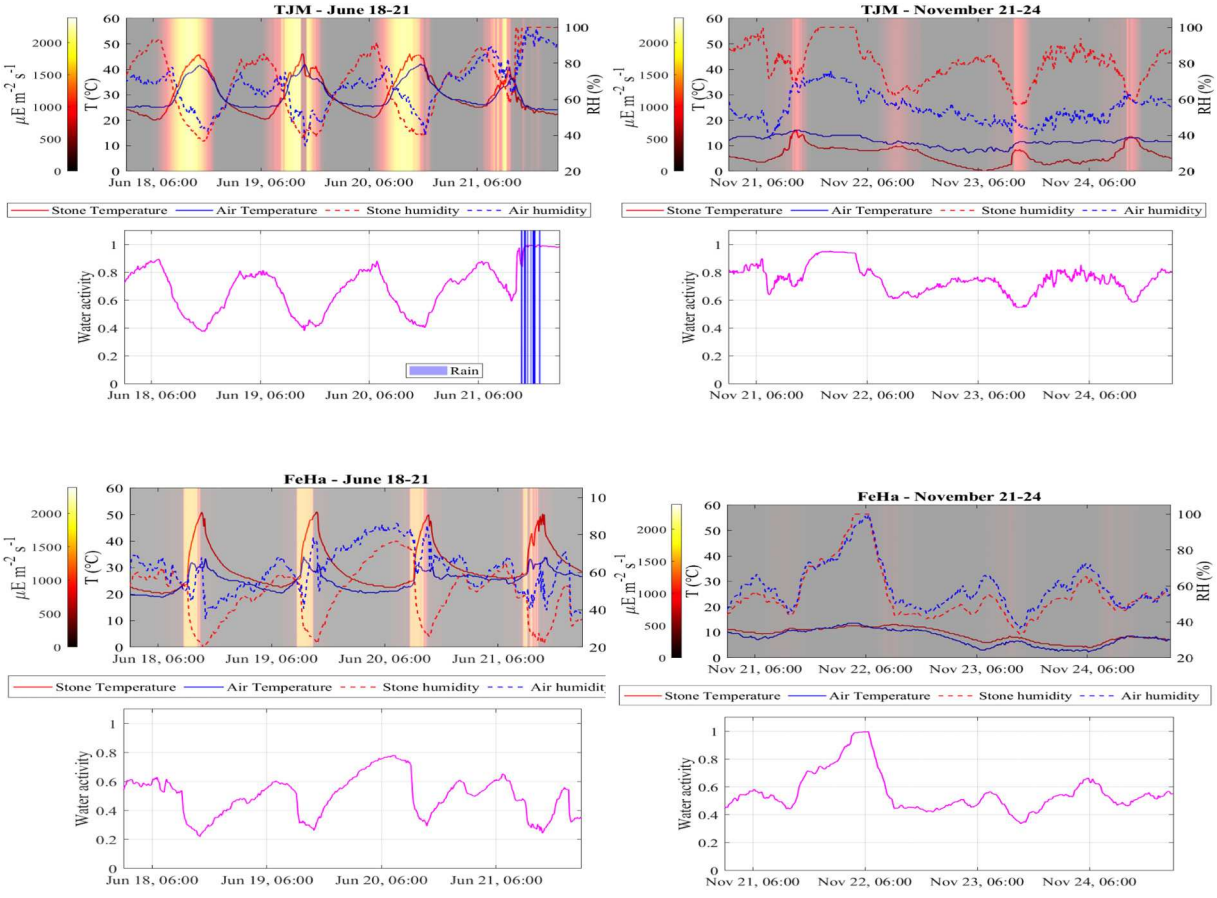

Fig. 6. Representative temperature, relative humidity, and light intensity data, as well as computation of SAB water activity (at SAB thickness $h = 15\mu$m) for TJM (top 4 subfigures) and FH (bottom 4 subfigures). (Red solid) stone temperature, (blue solid) ambient air temperature away from the stone surface, (black solid) estimated temperature at SAB-air interface, (red dash) RH at stone surface, (blue dash) RH in ambient air away from the stone surface, (magenta solid) computed water activity. Background colors indicate light intensity (μE s^{-1}m^{-2}). Note that rain events are indicated by vertical blue bars.

4. Results and discussion

To better understand how and when SABs obtain water, an approximately year-long data gathering campaign was conducted on the marble roofs of the portico of TJM and of FH, tracking temperature (on the surface of the stone as well as of nearby ambient air), moisture (rainfall as well as relative humidity, with the latter measured on the surface of the stone), and light intensity. See Supplemental Material for the full data set. Temperature and humidity measurements for representative weather data for both TJM and FH locations) are shown in Fig. 6. The bacterial communities of both TJM and FH were surveyed using standard methods (see Supplemental Material) and were found to be dominated by members of the phylum Cyanobacteria (TJM 71.9 %; FH 87.7 %) with a notable percentage of Actinobacteria (TJM 10.5 %; FH 7.2 %), Proteobacteria (TJM 10.4 %; FH 2.0 %) and Deinococcus-Thermus (TJM 3.5 %; FH 0.9 %), indicating the presence of a phototrophically-driven SAB. Note that, at least at the phylum level, the two communities appear relatively similar, as also do their SAB thicknesses (see Fig. 3).

Fig. 7 shows averages, by season, of the difference $T_a - T_s$ of ambient air temperature with stone temperature, again as a function of time of day. Larger values are indicators for larger relative humidities close to the SAB. Note the favorability for early morning times, especially noticeable at TJM. To quantitate this observation, we used measured data (temperatures and relative humidities) to solve eqs. (6) and (8) for water activity a_w; see Fig. 8 for seasonally averaged water activity as a function of time of day (the diel cyclic behavior of water activity is noticeable in Fig. 6). Observe again the favorability of early morning hours, particularly in warmer seasons. Also note the reduced light intensities as well as reduced ambient air vs stone temperatures at FH, both likely a consequence of the urban canyon environment of FH. As a consequence, higher values of water activity are estimated at TJM vs FH. Additional illustration including seasonal behavior can be found in the Supplemental Material.

See Fig. 9 for computed water activity frequency, obtained by averaging over the entire, approximately year-long, data set, again for both locations, based on a 15 μm thick SAB. (Measurements of SAB thickness h averaged approximately 14 μm in both locations, see Fig. 3, with 15 μm inside the one sigma interval for both locations.) A recent survey of water activity for survival of low water activity tolerant microbes estimates minimum $a_w \approx 0.6$, though growth is generally inhibited, even for xerophiles, as water activity passes through the range $0.69 < a_w < 0.85$ (Stevenson et al., 2015). Cyanobacteria have been shown able to actively grow at water activities at least as low as $a_w \approx 0.78$ in brine (Oren, 2012), close to the minimum possible water activity in such systems; we are not aware of corresponding data for SABs. (It is worth mentioning, though, that observations of desiccated cyanobacterial SABs indicate that significant rehydration occurs at RH ≈ 70% or higher (Davila and Gómez-Silva, 2008, Villa et al., 2015), which, coincidentally, is close to the known lower limits for microbial viability.) Note that the model predicts that FH and TJM sites regularly see water activities above 0.70 during morning hours, see Fig. 9, supporting the hypotheses that communities at both sites have consistent access to sufficiently active water as to allow long-term survival. Interestingly, despite higher water activity at TJM, its SAB thickness is not significantly different from that at FH, suggesting water activity is not by itself determinative for microbial community thickness at least at the two sites studied, though it might influence overall biofilm mass in terms of stone coverage area.

Maximal liquid water activity, generally, occurs in the early morning hours when T_a is typically near a daily minimum and $T_a - T_s$ is typically at a daily maximum. This effect is tied to heat reservoir properties of stone. Note that light intensity levels during the early morning time period are low to moderate which also may be advantageous – high light intensity can in fact be damaging (El Moustaid et al., 2017; Falkowski and Raven, 2007), even in winter. Note also that data from leaf-wetness sensors placed near to the temperature and relative humidity sensors does not indicate similar daily signals (see Supplemental Material), also supporting the inference that stone properties such as albedo and heat storage capacity are important (leaf-wetness sensors were placed near to the stone but outside of the thermal boundary layer, and are sufficiently thin as to allow their temperatures to equilibrate with the surrounding ambient air, unlike nearby stone surfaces).

Liquid water limited, not to mention free water limited, environments are perhaps surprisingly common, and microbial communities are often important components in these systems, e.g., both warm and cold deserts (Kennedy, 1993). SABs can extract liquid water from water vapor, even at relatively low relative humidity through a generalized osmotic tension generated for example by hydrophilic properties of the SAB-stone system (e.g., Wierzchos et al., 2006). This tension is difficult to measure directly and may be variable from system to system. We argue here, though, that resulting steady state water activity is essentially independent of generalized osmotic tension, though, and is fundamentally determined by local environmental conditions. The assumption of steady state is important however, and it should be noted that we don't exclude the possibility that SABs can temporarily influence water activity by manipulating approach to steady state.

To summarize, (Adhikary and Kovacik, 2010) temperature and relative humidity measurements from stone monuments can be used to predict daily and seasonal steady state water activity values in SABs. (Alduchov and Eskridge, 1997) SABs may be able to affect their water content but, at least at steady state, cannot directly change water

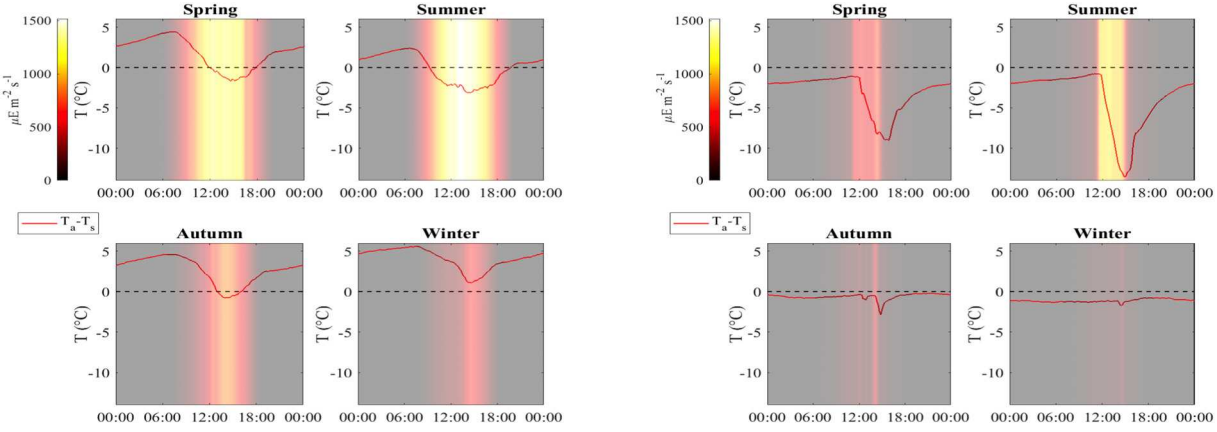

Fig. 7. Difference between ambient air and stone temperature. Averaged difference in ambient air vs stone temperature (ambient air temperature – stone temperature) by season, TJM (left) and FH (right) by season.

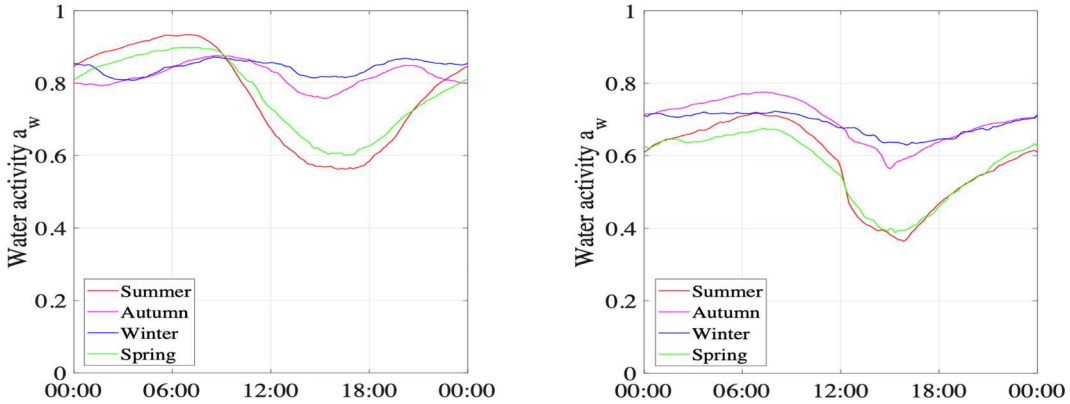

Fig. 8. Water activity. Water activity according to time to day, averaged by season, computed for an SAB of thickness $h = 15\mu$m. TJM (left) and FH (right).

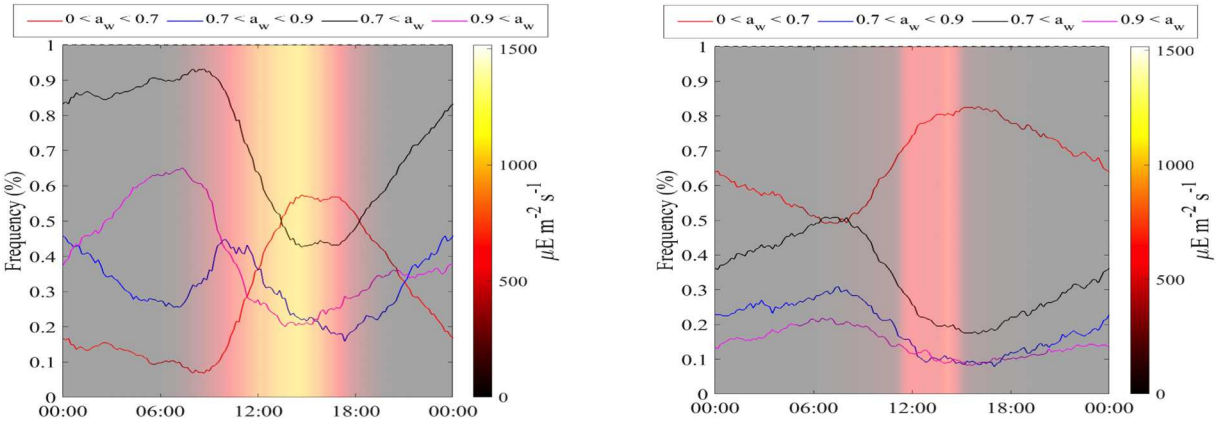

Fig. 9. Water activity a_w vs time of day, averaged over the entire TJM (left) and FH (right) data sets, for a SAB of thickness $h = 15\mu$m. (Red) average frequency that $a_w < 0.7$, (blue) average frequency that $0.7 < a_w < 0.9$, (magenta) average frequency that $0.9 < a_w$, (black) average frequency that $0.7 < a_w < 1$. Average frequency is here defined as the number of measurement days on which the event occurs at a specific time, relative to the total number of measurement days. Red, blue, and magenta curves sum to one. Background colors indicate light intensity (μE s^{-1}m^{-2}). The data suggests that morning is optimal for community activity.

activity which is, rather, determined by relative humidity. This matters, as higher water activity assists metabolic activity. (Allen Jr., 2018) Relative humidity of air, for a given water content, depends on temperature. Since ambient air temperature can differ from air temperature directly adjacent to a stone surface, so can relative humidity. Though this is a known observation, it is still worth highlighting (Alves et al., 2021). Lower temperature for a given water content implies higher relative humidity. Stone temperature tends to be lowest, relative to ambient air temperature, during early morning hours. As a consequence, mathematical modeling predicts that early morning may be optimal for water activity and hence for SAB activity.

5. Conclusions

Free, liquid water is an essential requirement for microbial growth and activity, and its availability can be effectively assessed through water activity. Stone monuments exemplify extreme ecosystems where high activity liquid water is not always readily accessible (Villa et al., 2016; Villa and Cappitelli, 2019). However, SABs that colonize lithic surfaces manage to thrive in such xeric environments nonetheless. Water activity is ultimately a physical concept, though, so understanding its physical limits is thus relevant for environmental science and conservation practice; the consequences of microbial activities have far-reaching implications for ecosystem services (Sanmartin et al., 2023) and the mechanisms by which stone monuments deteriorate (Liu et al., 2022).

It is natural to focus on SAB acquisition of liquid water, and, to date, a few specific mechanisms have been described, including salt deliquescence (Wierzchos et al., 2006; Davila, 2013; Villa et al., 2023) and the extraction of crystallization water from rocks (Huang et al., 2020). Here, rather, for the first time, we explore the general consequences of physical/chemical processes that allow SABs to extract liquid water from the atmosphere, regardless of the microbial community composition and the surface type. With the help of a mathematical model, we present evidence to support the notion that steady state water activity within SABs is significantly constrained by local environmental conditions, independent of details of the water recovery mechanisms generated by the biofilm itself. Further, we present a methodology to estimate SAB water activity that can be achieved with minimally invasive collection methods by taking into account simple and readily available data such as the local temperature, relative humidity, and SAB thickness.

The results presented here are intended to address existing knowledge gaps concerning water activity in biofilms across diverse environmental conditions, and provide a tool for better understanding biofilms on stone monuments and their erosive or protective function, and possible means to reduce their presence. Further, it is worth noting that, being independent of microbial community composition and of substrate type, the applicability of our methods extends to a wide range of settings and objects including paintings, library collections, and artifacts; managers of cultural heritage can be assisted in monitoring and addressing potential microbial risks and designing effective preservation strategies in order to better safeguard all monuments, objects, and collections.

We also argue that a focus on a physical viewpoint is necessary for understanding SAB response to climate change. There is a significant likelihood of intensified drought conditions in numerous regions. These changes have the potential to disrupt the global water cycle, which in turn affect water conditions in the atmosphere (Sherwood et al., 2018). In this context, understanding the connections between water activity in SABs and changing temperature and relative humidity becomes paramount. In doing so, we not only gain insights into SAB response to climate change and their impact on the underlying substrates, but also improve our understanding of the potential for resistance and resilience of these microbial communities in the face of environmental shifts.

Author contributions

D. Bitterman: Investigation.
B. Buttaro: Methodology, Supervision.
F. Villa: Investigation, Writing.
J. Jacob: Investigation.
I. Klapper: Methodology, Supervision, Writing.
A. Tenore: Investigation, Methodology, Writing.
Y. Wu: Investigation.

Declaration of competing interest

The authors declare that they have no known competing financial interests or personal relationships that could have appeared to influence the work reported in this paper.

Data availability

Data is shared in Supplemental Material

Acknowledgments

The authors wish to thank the US National Park Service for the assistance and to acknowledge support from NSF awards 1517100 and 1951532.

Appendix A. Supplementary data

Supplementary data to this article can be found online at https://doi.org/10.1016/j.scitotenv.2023.165790.

References

Adhikary, S.P., Kovacik, L., 2010. Comparative analysis of cyanobacteria and microalgae in the biofilms on the exterior of stone monuments in Bratislava, Slovakia and in Bhubaneswar, India. J. Indian Bot. Soc. 89, 19–23.
Alduchov, O.A., Eskridge, R.E., 1997. Improved Magnus Form Approximation of Saturation Vapor Pressure (US Department of Energy Technical Report DOE/ER/61011-T6). https://doi.org/10.2172/548871.
Allen Jr., L.V., 2018. Quality Control: Water Activity Considerations for beyond-Use Dates. Int J Pharm Compd 22, 288–293. 30021184.
Alves, C.C., Figueiredo, C.A.M., Sanjurjo-Snchez, J., Hernndez, A.C., 2021. Effects of water on natural stone in the built environment: a review. Geosciences 11, 459. https://doi.org/10.3390/geosciences11110459.
Benison, K.C., O'Neill, W.K., Blain, D., Hallsworth, J.E., 2021. Water activities of acid brine lakes approach the limit for life. Astrobiology 21, 729–740.
Brown, A.D., 1990. Microbial Water Stress Physiology. John Wiley & Sons, Chichester.
Davila, A.F., 2013. I, Hawes, C, Ascaso, J, Wierzchos, salt deliquescence drives photosynthesis in the hyperarid Atacama Desert. Environ. Microbiol. 5, 583–587.
Davila, A.F., Gómez-Silva, B., de los Rios, A., Ascaso, C., Olivares, H., McKay, C.P., Wierzchos, J., 2008. Facilitation of endolithic microbial survival in the hyperarid core of the Atacama Desert by mineral deliquescence. J. Geophys. Res. 115, G01028.
P.R. Day, G.H. Bolt, D.M. Anderson, Nature of soil water, R.M. Hagan, H.R. Haise, T.W. Edminster (eds.), *Irrigation of agricultural lands*, 193–208, Am. Soc. Agron., Madison, WI. (1967).
El Moustaid, F., Carlson, R.P., Villa, F., Klapper, I., 2017. Photorespiration and rate synchronization in a phototroph-heterotroph microbial consortium. Processes 5. https://doi.org/10.3390/pr5010011.
Falkowski, P.G., Raven, J.A., 2007. Aquatic Photosynthesis. Princeton University Press, Princeton.
Flemming, H.C., van Hullebusch, E.D., Neu, T.R., et al., 2023. The biofilm matrix: mulptasking in a shared space. Nat Rev Microbiol 21, 70–86. https://doi.org/10.1038/s41579-022-00791-0.
Gaylarde, C.C., Rodriguez, C.H., Navarro-Noya, Y.E., Ortega-Morales, B.O., 2012. Microbial biofilms on the sandstone monuments of the Angkor Wat complex, Cambodia. Curr. Microbiol. 64, 85–92.
Gorbushina, A.A., 2007. Life on the rocks. Environ. Microbiol. 9, 1613–1631.
Huang, W., Ertekin, E., Wang, T., Cruz, L., Dailey, M., DiRuggiero, J., Kisailus, D., 2020. Mechanism of water extraction from gypsum rock by desert colonizing microorganisms. Biolog Sci 117, 10681–10687.
Kennedy, A.D., 1993. Water as a limiting factor in the antarctic terrestrial environment: a biogeographical synthesis. Arct. Antarct. Alp. Res. 25, 308–315. https://doi.org/10.1080/00040851.1993.12003017.
Lange, O.L., Meyer, A., Budel, B., 1984. Net photosynthesis activation of a desiccated cyano-bacterium without liquid water in high air humidity alone. Experiments with *Microcoleus sociatus* isolated from a desert soil crust. Funtional Ecology 8, 52–57. https://doi.org/10.2307/2390111.
Li, Y.-H., Gu, J.-G., 2022. A more accurate definition of water characteristics in stone materials for an improved understanding and effective protection of cultural heritage from biodeterioration. Int. Biodeterior. Biodegradation 166, 105338. https://doi.org/10.1016/j.ibiod.2021.105338.
Liu, X., Koestler, R.J., Warscheid, T., et al., 2020. Microbial deterioration and sustainable conservation of stone monuments and buildings. Nat Sustain 3, 991–1004. https://doi.org/10.1038/s41893-020-00602-5.
Liu, X., Qian, Y., Wu, F., Wang, Y., Wang, W., Gu, J.D., 2022. Biofilms on stone monuments: biodeterioration or bioprotection? Trends Microbiol. 30, 816–819.
McNamara, C.J., Mitchell, R., 2005. Microbial deterioration of historic stone. Front. Ecol. Environ. 3, 445–451.
Nobel, P.S., 2020. Physicochemical and Environmental Plant Physiology, 5th edition. Academic Press.
Ollion, J., Cochennec, J., Loll, F., Escudé, C., Boudier, T.T., 2013. TANGO: a generic tool for high-throughput 3D image analysis for studying nuclear organization. Bioinformatics 29, 1840–1841.
Oren, A., 2012. In: Whitton, B.A. (Ed.), "Salts and Brines" in *Ecology of Cyanobacteria II: Their Diversity in Space and Time*. Springer, Dordrecht.
Potts, M., 1994. Desiccation tolerance of prokaryotes. Microbiol. Rev. 58, 755–805.
Quan, K., Hou, J., Zhang, Z., Ren, Y., Peterson, B.W., Flemming, H.-C., Mayer, C., Busscher, H.J., van der Mei, H.C., 2022. Water in bacterial biofilms: pores and channels, storage and transport functions. Crit. Rev. Microbiol. 48, 283–302. https://doi.org/10.1080/1040841X.2021.1962802.
Rasband, W.S., 2018. ImageJ, U.S. National Institutes of Health. Bethesda, Maryland, USA. https://imagej.nih.gov/ij/ (1997-2018).
Rödel, W., 2001. Water activity and its measurement in food. In: Instrumentation and Sensors for the Food Industry, pp. 453–483. https://doi.org/10.1533/9781855736481.2.453.
Sanmartin, P., Bosch-Roig, P., Pangallo, D., et al., 2023. Unraveling disparate roles of organisms, from plants to bacteria, and viruses on built cultural heritage. Appl. Microbiol. Biotechnol. 107, 2027–2037. https://doi.org/10.1007/s00253-023-12423-5.
Sass, O., Viles, H., 2022. Heritage hydrology: a conceptual framework for understanding water fluxes and storage in built and rock-hewn heritage. Heritage Science 10 (66), 2022. https://doi.org/10.1186/s40494-022-00693-7.
Schlichting, H., 1955. Boundary-Layer Theory. McGraw-Hill Book Company, New York.
Sherwood, S.C., Dixit, V., Salomez, C., 2018. The global warming potential of near-surface emitted water vapour. Environ. Res. Lett. 13, 104006.
Song, M.-A., Kim, O.-J., Lee, O.-M., 2012. The distribution and ecological factors of aerial algae inhabiting stoneworks in Korea. The Korean Society of Phycology 27, 283–294.
Stevenson, A., Burkhardt, J., Cockell, C.S., Cray, J.A., Dijksterhuis, J., Fox-Powell, M., Kee, T.P., Kminek, G., McGenity, T.J., Timmis, K.N., Timson, D.J., Voytek, M.A., Westall, F., Yakimov, M.M., Hallsworth, J.E., 2015. Multiplication of microbes below 0.690 water activity: implications for terrestrial and extraterrestrial life. Environ. Microbiol. 17, 257–277.
Stupar, M., Grbić, M.L., Simić, G.D., Jelikić, A., Vukojević, J., Savbovlejić, M., 2012. A sub-aerial biofilms investigation and new approach in biocide application in cultural heritage conservation: holy virgin church (Gradac monastery, Serbia). Indoor Built Environ 23, 584–593.
Sutherland, I.W., 2001. The biofilm matrix – an immobilized but dynamic microbial environment. Trends Microbiol. 9, 222–227. https://doi.org/10.1016/s0966-842x(01)02012-1.
Videla, H.A., Guiamet, P.S., Gomez de Saravia, S., 2000. Biodeterioration of Mayan archaeological sites in the Yucatan Peninsula, Mexico. Int Biodet Biodegr 46, 335–341.
Villa, F., Cappitelli, F., 2019. The ecology of subaerial biofilms in dry and inhospitable terrestrial environments. Microorganisms 7, 380. https://doi.org/10.3390/microorganisms7100380.
Villa, F., Pitts, B., Lauchnor, E., Cappitelli, F., Stewart, P.S., 2015. Development of a laboratory model of a phototroph-heterotroph mixed-species biofilm at the stone/air interface. Front. Microbiol. 6, Article 1251.
Villa, F., Stewart, P.S., Klapper, I., Jacob, J.M., Cappitelli, F., 2016. Subaerial biofilms on outdoor stone monuments: changing the perspective toward an ecological framework. Bioscience 66, 285–294.
Villa, F., Ludwig, N., Mazzini, S., Scaglioni, L., Fuchs, A.L., Tripet, B., Copié, V., Stewart, P.S., Cappitelli, F., 2023. A desiccated dual-species subaerial biofilm reprograms its metabolism and affects water dynamics in limestone. Sci. Total Environ. 868, 161666.

Wierzchos, J., Ascaso, C., McKay, C.P., 2006. Endolithic cyanobacteria in halite rocks from the hyperarid core of the Atacama desert. Astrobiology 6, 415–422.
Zanardini, E., May, E., Purdy, K.J., 2018. Nutrient cycling potential within microbial communities on culturally important stoneworks. Environ. Microbiol. 11, 147–154. https://doi.org/10.1111/1758-2229.12707.
Zhang, T., Klapper, I., 2010. Mathematical model of biofilm induced calcite precipitation. Wat. Sci. Tech. 61, 2957–2964.
Zippel, B., Neu, T.R., 2011. Characterization of glycoconjugates of extracellular polymeric substances in tufa-associated biofilms by using fluorescence lectin-binding analysis. Appl. Environ. Microbiol. 77, 505–516.